Paleoceanography and Paleoclimatology®

Key Points:

- We applied the LDI as a paleothermometer to sedimentary records from the Arabian Sea focusing on the last glacial–interglacial transition
- The sea surface temperature records showed decreasing values with the onset of the deglaciation, different from other proxy records
- Strong upwelling may cause this cold bias, which was observed particularly at one record, offshore Oman

Supporting Information:

Supporting Information may be found in the online version of this article.

Correspondence to:

Z. Erdem,
zeynep.erdem@nioz.nl

Author Contributions:

Conceptualization: G.-J. Reichart, J. S. Sinninghe Damsté, S. Schouten
Data curation: M. R. van Erk, E. Mezger, A. Lückge
Formal analysis: E. Mezger
Funding acquisition: G.-J. Reichart, S. Schouten
Investigation: J. Lattaud, M. R. van Erk, E. Mezger
Methodology: J. Lattaud, E. Mezger
Project Administration: G.-J. Reichart, S. Schouten
Resources: G.-J. Reichart, A. Lückge, S. Schouten
Supervision: G.-J. Reichart, J. S. Sinninghe Damsté, S. Schouten
Writing – original draft: S. Schouten

Applicability of the Long Chain Diol Index (LDI) as a Sea Surface Temperature Proxy in the Arabian Sea

Z. Erdem[1] , J. Lattaud[1,2] , M. R. van Erk[1,3], E. Mezger[1], G.-J. Reichart[1,4] , A. Lückge[5], J. S. Sinninghe Damsté[1,4], and S. Schouten[1,4]

[1]NIOZ Royal Netherlands Institute for Sea Research, Texel, The Netherlands, [2]ETH Zurich, Zurich, Switzerland, [3]Max Planck Institute for Marine Microbiology, Bremen, Germany, [4]Utrecht University, Faculty of Geosciences, Utrecht, The Netherlands, [5]Bundesanstalt für Geowissenschaften und Rohstoffe, Hannover, Germany

Abstract The long-chain diol index (LDI) is a relatively new proxy for sea surface temperature (SST) which has been rarely applied in upwelling regions. Here, we evaluated its application by comparison with other SST records obtained by commonly used proxies, that is, the Mg/Ca ratio of the planktonic foraminifera species *Globigerinoides ruber* and the alkenone paleothermometer $U^{K'}_{37}$. We focused on the last glacial–interglacial transition of four different sedimentary archives from the western and northern Arabian Sea, which are currently under the influence of monsoon-induced upwelling and the associated development of an oxygen minimum zone. The $U^{K'}_{37}$ and $Mg/Ca_{G.ruber}$ SST records revealed an increase of 0.6–3.4°C from the Last Glacial Maximum to the late Holocene with somewhat higher amplitude in the northern part of the Arabian Sea than compared to the western part. In contrast, the LDI SSTs did not reveal major changes during the last glacial–interglacial transition which was followed by a decreasing trend during the Holocene. The LGM versus the Holocene LDI SSTs ranged between −0.2 and −2.7°C. Particularly at one record, offshore Oman, the SST decrease during the Holocene was high in amplitude, suggesting a potential cold bias, possibly related to changes in upwelling intensity. This indicates that care has to be taken when applying the LDI for annual mean SST reconstruction in upwelling regions.

1. Introduction

Reconstructing past ocean temperature is essential for understanding past climate change, its drivers, and responsible mechanisms. Several proxies were established over the past decades in order to reconstruct sea surface temperature (SST) and changes therein. Planktonic foraminiferal assemblages (by transfer function (Imbrie & Kipp, 1971; Pflaumann et al., 1996), stable oxygen isotopes ($δ^{18}O$) (Erez & Luz, 1983; Urey et al., 1954), and Mg/Ca ratios of planktonic foraminifera species (Elderfield & Ganssen, 2000; Nürnberg et al., 1996) and organic proxies, such as the $U^{K'}_{37}$ index (Brassell et al., 1986; Prahl & Wakeham, 1987) based on the long chain alkenones synthesized by haptophyte algae, have been widely applied as paleo-thermometers. However, discrepancies between various SST proxy records as well as with SST reconstructions based on climate model simulations have been observed. This is particularly the case concerning the reconstructed Last Glacial Maximum (LGM) SSTs reported in the tropical oceans and the upwelling regions where proxy records and models show disagreement with each other as well as with global estimates (e.g., Kucera et al., 2005; Mix et al., 2001; Shakun et al., 2012; Waelbroeck et al., 2009). Accordingly, there is a need for an increased fundamental understanding of the processes that control the imprint of temperature on these proxies as well as the processes underlying the observed offsets.

In the last decade, the LDI (Long-chain Diol Index; Rampen et al., 2012), which is based on the distribution of certain long-chain diols (LCDs), has been developed. The LDI is based on the relative abundances of 1,13- and 1,15-diols of which culture studies showed that they are produced by freshwater and marine eustigmatophyte algae. However, in the marine realm, it is still uncertain what the source organisms are (e.g., Balzano et al., 2018; Rampen et al., 2014; Volkman et al., 1992; Volkman et al., 1999). The number of studies of late Quaternary LDI applications has been rapidly increasing recently (Dauner et al., 2019; de Bar et al., 2018; Häggi et al., 2019; Jonas et al., 2017; Lattaud et al., 2018; Lopes dos Santos et al., 2013; Rodrigo-Gámiz et al., 2015; Warnock et al., 2018; Zhu et al., 2018) giving broader information on global SST variations in the past. Recently, a more extended calibration for the LDI became available, providing further insight into the main constraints on its applicability (de Bar et al., 2020). Overall, the new calibration dataset was in line with downcore applications but also showed that (i) the LDI has limitations in certain regions, such as in the front of river mouths, in low salinity

Writing – review & editing: J. Lattaud,
M. R. van Erk, G.-J. Reichart, A. Lückge,
J. S. Sinninghe Damsté, S. Schouten

regions, and at high latitudes; (ii) the abundance of LCDs other (e.g., 1,12 and 1,14-diols) than those used for the LDI may indicate a cold bias of LDI-derived SST estimations. It was, therefore, suggested to use other LCD-based indices [e.g., diol upwelling index (DI) and the relative abundance of C_{28} 1,12-diol (FC_{28} 1,12-diol)] prior to LDI applications to constrain potential biases (de Bar et al., 2020). However, many uncertainties with respect to the application of the LDI still remain, such as those related to changing nutrient regimes, seasonality, and other potential changes in the water column (e.g., mixed layer depth, oxygenation). Moreover, SST reconstructions from (sub)tropical upwelling regions indicated discrepancies and uncertainties between proxies and modeling approaches (e.g., Otto-Bliesner et al., 2009). Multi-proxy approaches can, therefore, be helpful to constrain these uncertainties (Kucera et al., 2005; Mix et al., 2001; Waelbroeck et al., 2009) as well as to better our understanding of past climate in tropical upwelling regions.

Here, for the first time, we applied the LDI to generate four SST records from different locations in the Arabian Sea focusing on the last glacial-interglacial period. The Arabian Sea is characterized by strong upwelling conditions dependent on monsoon activity, particularly in the west, with relatively warm surface waters during the year [24–27°C Arabian Sea (Locarnini et al., 2013)]. The Arabian Sea has been the focus of studies on past SST reconstructions for more than two decades (e.g., Böll et al., 2015; Doose-Rolinski et al., 2001; Emeis et al., 1995; Gaye et al., 2018; Huguet et al., 2006a; Ivanochko et al., 2005; Rostek et al., 1997; Schulz et al., 1998; Sonzogni et al., 1998). These studies have revealed contrasting trends and magnitudes of SST changes as reconstructed by various proxies as well as simulated using state-of-the-art climate models, particularly concerning the last glacial-interglacial transition. Application of the foraminifera transfer function suggested that the western Arabian Sea experienced almost no cooling during the LGM (CLIMAP Project, 1981), whereas the alkenone paleothermometer indicated 1–4°C warming between LGM and the late Holocene (Sonzogni et al., 1998). Moreover, modeling approaches reported a variable LGM SST range (1–3°C cooler compared to modern-day) for the Arabian Sea (Mix et al., 2001; Otto-Bliesner et al., 2009; Waelbroeck et al., 2009). The disagreement between proxy-based estimations has been related to organisms' habitats as well as to regional environmental changes (e.g., Dahl & Opp, 2006; Rosell-Melé et al., 2004; Sonzogni et al., 1998) and has been recognized as a common issue in the SST reconstruction of the LGM-Holocene warming in tropical regions (e.g., Waelbroeck et al., 2009). In this study, our aim is to test the applicability of the LDI using four sedimentary records recovered from the western and northern Arabian Sea by comparing the obtained reconstructed SST records with other SST proxy estimates from the same cores and evaluate the potential application of the LDI in a tropical upwelling region.

2. Research Setting

In the Arabian Sea, the seasonal cycle is regulated by the Indian monsoon, which is driven by the pressure gradient between the Tibet Plateau and the South Indian Ocean (Rixen et al., 2000; Webster et al., 1998; Wyrtki, 1973). Low temperatures over the Tibetan Plateau and the Himalayas in boreal winter (January–March) cause a high-pressure system over Central Asia and hence a strong pressure gradient toward the low-pressure cell located in the Indian Ocean. During this period, dry and cold northeasterly winds prevail over the Arabian Sea, resulting in cooler surface waters (Webster et al., 1998), particularly in the north of the Arabian Sea (Figure 1a). During boreal summer (July–September), a strong pressure gradient between the Indian-Tibetan low-pressure cell and a high-pressure belt over the Southern Ocean results in powerful southwesterly winds. During this southwest (SW) monsoon period, the Intertropical Convergence Zone (ITCZ) is positioned in the north (Figure 1b). As a result of these strong, warm, and humid SW winds, upwelling of nutrient-rich waters occurs along the margin of Oman to Somalia, leading to lower SSTs (24–25°C) in the western Arabian Sea in comparison with the rest of the region and annual mean SST (e.g., Haake et al., 1993; Locarnini et al., 2013; Wakeham et al., 2002). During the NE monsoon, the upwelling is suppressed, and waters above the thermocline are convectively mixed until the top of the oxygen minimum zone (OMZ) (Wakeham et al., 2002), as northernmost Arabian Sea exhibits 3–4°C cooling in the surface waters (Dahl & Oppo, 2006).

The Arabian Sea is one of the most productive open marine systems in the world today (Qasim, 1982; Smith et al., 1998). Whilst primary productivity has its annual maximum during the SW monsoon, particularly in the west due to enhanced upwelling, it is substantially less during the NE monsoon (Haake et al., 1993; Honjo et al., 1999; Wakeham et al., 2002). The combination of high productivity, subsequent mineralization of organic matter as it settles through the water column, and consumed dissolved oxygen together with sluggish ventilation of intermediate waters in the Arabian Sea results in one of the strongest OMZs in the world (e.g., Helly &
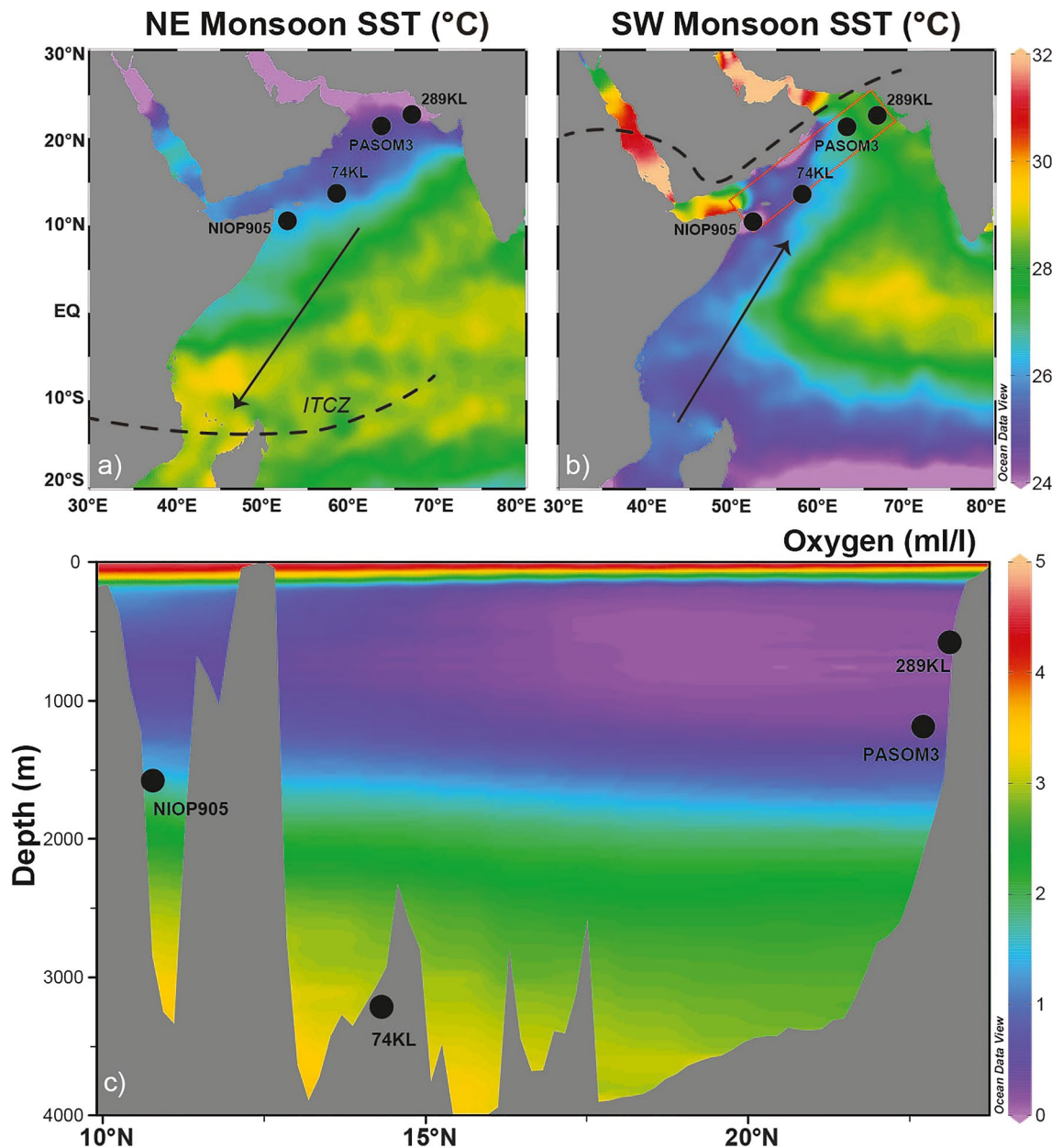
Figure 1. Maps of the Arabian Sea with sediment core locations showing (a) SST during Jan–Mar (NE Monsoon) and (b) SST during Jul–Sep (SW Monsoon). (c) A cross section of dissolved oxygen concentrations in the water column along the transect indicated by red box in (b) Dashed lines indicate the ITCZ position, and arrows show the wind direction. Data were obtained from the World Ocean Atlas (Garcia et al., 2013; Locarnini et al., 2013), and the figure was prepared using ODV (Schlitzer, 2015).

Levin, 2004; Paulmier & Ruiz-Pino, 2009; Wyrtki, 1971). The OMZ, defined as waters with oxygen concentrations <0.5 ml/l (~22 µM), is located in the Arabian Sea at water depths of ca. 150–1200 m (Figure 1c) (Acharya & Panigrahi, 2016; Helly & Levin, 2004; Olson et al., 1993; Sarma, 2002; Wyrtki, 1973). Despite the higher primary productivity and organic matter export to the deep sea in the western part of the region, the OMZ is much more pronounced in the northeast east (Acharya & Panigrahi, 2016; Naqvi, 1991; Rixen et al., 2014). This is mainly caused by the prevailing subsurface currents and intermediate water masses in the region, which is strongly influenced by the lack of an opening to the north. Ventilation of OMZ waters is facilitated by three water masses; First, high salinity Persian Gulf Water (PGW) in the north flowing south and eastwards (Prasad et al., 2001), second, less saline but denser Red Sea Water (RSW) flowing along the Oman coast (Shankar et al., 2005), and, third, oxygenated intermediate depth Indian Central Water (ICW) entering the Arabian Sea from the south. The

Table 1
Metadata of the Sediment Cores and References

Core Name	Core location Lat (N)	Core location Long (E)	Water depth (m)	Age model	$U^{K'}_{37}$	$\delta^{18}O_{G.ruber}$	$Mg/Ca_{G.ruber}$	LDI	$\delta^{15}N_{sed}$
NIOP905	10°47.0′	51°56.0′	1586	Huguet et al. (2006a)	Huguet et al. (2006a, 2006c)	Sirocko et al. (1993)	Anand et al. (2008)	This study	Ivanochko et al. (2005)
SO42-74KL	14°19.2'	57°20.8′	3212	Huguet et al. (2006a) [a]	Huguet et al. (2006a, 2006b)	Jung et al. (2001)	Dahl and Oppo (2006)	This study	Suthhof et al. (2001)
PASOM3	22°19.9′	63°36.0′	1172	This study	This study	This study	This study	This study	n.a.
SO130-289KL	23°07.3'	66°29.8′	571	Deplazes et al. (2013)	n.a.	n.a.	n.a.	This study	n.a.

[a]Age Model is Tuned (see Figure S1). n.a., not available.

ICW is initially rich in oxygen but by the time it reaches the Arabian Sea, it is oxygen depleted and nutrient-rich (Olson et al., 1993). Recently, it was shown that the influence of ICW in the region is observed predominantly during the SW Monsoon (Schmidt et al., 2020). The intense OMZ causes denitrification within the water column (Wyrtki, 1973) with strongest rates observed in the northeast–east Arabian Sea (Gaye-Haake et al., 2005), where the maximum expansion of the OMZ is observed (Figure 1c).

Sedimentary archives from the Arabian Sea suggest a teleconnection between the Indian monsoon and Northern Hemisphere (NH) climate variability (e.g., Böning & Bard, 2009; Clemens & Prell, 2003; Deplazes et al., 2013; Deplazes et al., 2014; Reichart et al., 1998; Reichart, Nortier, et al., 2002; Schulte & Müller, 2001; Schulz et al., 1998; Sirocko et al., 1996). Interstadials are generally characterized by an intensified Arabian Sea OMZ, while during stadials, the strength of the OMZ is substantially reduced (Altabet et al., 2002; Gaye et al., 2018; Pichevin et al., 2007; Reichart et al., 1998; Schulz et al., 1998). Meanwhile, proxy evidence has suggested contrasting differences in the west and east of Arabian Sea in terms of upwelling intensity and surface water productivity (e.g., Emeis et al., 1995; Schulte et al., 1999). Moreover, with the onset of the last deglaciation with interruptions during the cold periods, stronger SW Monsoon, intensified upwelling and enhanced productivity were reported in the records from the western Arabian Sea (Gaye et al., 2018; Marcantonio et al., 2001; Rampen et al., 2008; Singh et al., 2011; Sirocko et al., 1996).

3. Materials and Methods

3.1. Sediment Cores and Age Models

Four sediment cores were studied. They were collected from different areas during different expeditions; SO42-74KL (in 1986; Kasten core) and NIOP905 (in 1993; piston core) from western Arabian Sea, Oman–Somali upwelling zone; SO130-289KL (in 1998; Kasten core) and PASOM3 (in 2009; gravity core) from northern Arabian Sea within the OMZ from offshore Pakistan and the Murray Ridge, respectively (Figure 1, Table 1). The age models of cores NIOP905 and 74KL were published by Huguet et al. (2006a) and of core 289KL by Deplazes et al. (2013). We tuned the age model of core 74KL by fine-tuning of total organic carbon (TOC) to reflectance (L*) profile of core 289KL (Figure S1 in Supporting Information S1). This approach is based on previous observations, which show that the OMZ intensity has been synchronous basin wide, which was observed at both Oman and Pakistan Margins (Reichart, Schenau, et al., 2002), and cold periods are associated with lighter sediments (low TOC) and a high reflectance whereas warm periods are associated with darker sediments (high TOC) and lower reflectance (e.g., Deplazes et al., 2013; Schulz et al., 1998). The age model of core PASOM3 is primarily based on fine-tuning of L* data to the NGRIP (Andersen et al., 2004) and to L* profile of core 289KL (Text S1 in Supporting Information S1). In addition, three AMS radiocarbon ages, based on mixed planktonic foraminifera species (predominantly that belong to genus *Orbulina*) were determined (Beta Analytic Inc., USA). Calibrated ages (cal kyr BP; 0 BP equivalent to 1950 AD) were calculated using the conventional radiocarbon ages and the Marine13 calibration curve (Reimer et al., 2013). A regional reservoir age of 232 ± 26 years was applied according to the CALIB 7.1 database (Stuiver et al., 2017). The final correlation was based on a total of

41 tie points, and the age model was constructed by linear interpolation between these control points. The abundance of the deep-dwelling planktonic foraminifera *Globorotalia truncatulinoides* and *G. crassaformis* was used as an independent verification of the age model and was based on the existence of so-called *Globorotalia* events (Reichart et al., 1998).

3.2. *Globigerinoides Ruber* δ¹⁸O and Mg/Ca Analysis of Core PASOM3

For elemental and isotopic analysis, 50 specimens of *G. ruber* were hand-picked per sample from 250 to 355 μm fraction. Picked material was later crushed and divided into two parts; one third was saved for stable isotope analysis, and the remaining part was used for analyses of the elemental composition. The crushed foraminiferal specimens were cleaned following the Barker protocol (Barker et al., 2003) without the reductive cleaning step. This cleaning protocol includes removing clay particles using ultrapure water, ultrasonication and methanol, and removal of organic particles using an alkali buffered 1% H_2O_2 solution with NH_4OH. For elemental analysis, the same cleaning procedure and two additional cleaning steps were performed, including a reductive cleaning step for removal of metal-oxides (Fe, Mn) and a leaching procedure to remove adsorbed ions (Barker et al., 2003). Stable oxygen (δ¹⁸O) isotope analyses were performed using an automated carbonate device (Kiel IV, Thermo) connected to a Thermo Finnigan MAT 253 Dual Inlet IRMS. Values are reported in permille relative to the Peedee belemnite (PDB) standard in δ notation. For calibration, we used NBS19 (limestone) and in-house standard for drift detection (NFHS-1 (Mezger et al., 2016), showing a precision better than 0.1‰ for δ¹⁸O. Measurements for foraminiferal Mg/Ca composition were performed on an Element 2-ICPMS using low mass resolution. Samples were measured against four ratio calibration standards with a similar matrix and with a drift standard (NFHS-1) measured on every third sample. The monitor standards JCt-1 and NFHS-1 were measured for quality control (Mezger et al., 2016; Okai et al., 2002). The relative standard deviation (RSD 1-sigma) was around 0.8%. Additional quality control for potential contamination was done through molar ratios of Fe, Mn, Al, and Ca (mmol/mol) following Johnstone et al. (2016) and Lear et al. (2015). Overall, our results showed values below suggested thresholds (0.2 mmol/mol for Fe/Ca, 0.3 mmol/mol for Al/Ca, 0.1 mmol/mol for Mn/Ca) except one sample which is excluded from the results. The Mg/Ca SST were calculated using calibration of Anand et al. (2008) with calibration error of ca. 1.5°C.

3.3. Long Chain Diol and Alkenone Analysis

For LCD analysis, we extracted sediments obtained from cores PASOM3 and 289KL. For cores NIOP905 and 74KL, we analyzed the polar fractions previously obtained by Huguet et al. (2006a). For PASOM3 and 289KL, freeze-dried and homogenized sediments (9–18 g from PASOM3 and 0.75–11 g from 289KL) were extracted using an Accelerated Solvent Extractor 350 (ASE 350, DIONEX; 100°C and 7.6 × 106 Pa) and subsequently separated over an activated Al_2O_3 column into apolar, ketone, and polar fractions. The solvents hexane:DCM 9:1 (*v:v*), hexane:DCM 1:1 (*v:v*), and DCM:MeOH 1:1 (*v:v*) were used to elute the apolar, ketone, and polar fractions, respectively. Ketone fractions were used for alkenone analysis of PASOM3 that were conducted on a Hewlett Packard 6890 gas chromatograph (GC) equipped with a flame ionization detector (FID) and helium as the carrier gas, with an autosampler and an injection volume of 1 μL after re-dissolving the ketone fractions in 100–800 μL ethyl acetate. Separation was achieved on a fused silica column CP Sil-5 (50 m × 0.32 mm; film thickness 0.12 μm). Initial oven temperature of 70°C increased with 20°C per min to 200°C and subsequently with 3°C per min to 320°C, a temperature which was held for 25 min. Peak areas of $C_{37:2}$ and $C_{37:3}$ alkenones were determined by integration. The $U_{37}^{K'}$ values were calculated using the calibration of Müller et al. (1998) with a calibration error of 1.5°C and after the equation described by Prahl and Wakeham (1987):

$$\text{with } U_{37}^{K'} = [C_{37:2}]/([C_{37:2}] + [C_{37:3}]) \qquad (1)$$

For LCD analysis, polar fractions were silylated by the addition of 15 μL pyridine and 15 μL BSTFA, followed by heating at 60°C for 30 min. The analysis was carried out using an Agilent 7990B GC coupled to an Agilent 5977A MS following de Bar et al. (2017). The GC was equipped with an on-column injector and fused silica column (25 m × 0.32 mm) coated with CP Sil-5 (film thickness 0.12 μm). Samples were re-dissolved in 300–600 μL ethyl acetate, and the injection volume was 1 μL. The oven temperature was 70°C at injection and was programmed to increase to 130°C by 20°C/min, and subsequently to 320°C by 4°C/min, which was held for 25 min. Helium flow was held constant at 2 ml/min. The MS operated with an ionization energy of 70 eV and the temperature of the ion

Table 2
Modern Annual Mean SST Observed at the Site Location (Locarnini et al., 2013), SST Ranges, and SST Changes (ΔSST) Between the Last Glacial Maximum (19–22 kyr) and Late Holocene (0–5 kyr; Ca. 3–5 kyr for PASOM3, and 2–5 kyr for 289KL) Calculated for Each Core for Each Proxy

	Annual mean SST	$U^{K'}_{37}$ (°C)		LDI (°C)		$Mg/Ca_{G.ruber}$ (°C)	
Core name	Modern	Range	ΔSST	Range	ΔSST	Range	ΔSST
NIOP905	26.2	24.8–26.3	0.6	25.0–26.5	−0.5	22.7–25.6	1.7
SO42-74KL	26.5	24.8–27.4	2.0	21.1–26.0	−2.7	21.4–24.4	2.5[a]
PASOM3	26.7	20.4–26.8	3.4	24.4–26.3	−1.6	22.3–26.8	1.2
SO130-289KL	26.9	n.a.	n.a.	24.8–26.6	−0.2	n.a.	n.a.

[a]The values of ΔSST from the Mg/Ca ratio for core 74KL was calculated for time intervals of 24.3–24.5 kyr and 0.5–1.5 kyr after Dahl and Oppo (2006) considering the core depths reported in their study and the new age model reported in this study. Continuous downcore record of 74KL is not available. n.a.: not available.

source was 250°C and of the interface was 320°C. The total runtime was 75.5 min. Peak areas were defined using SIM of characteristic m/z ratios of LCD ions: 299.3 (C_{26} 1,12-diol and C_{28} 1,14-diol), 313.3 (C_{28} 1,13-diol and C_{30} 1,15-diol), 327.3 (C_{28} 1,12-diol and C_{30} 1,14-diol), and 341.3 (C_{30} 1,13-diol) (Rampen et al., 2012; Versteegh et al., 1997). Full-scan mode allowed for identity confirmation, since the different LCDs show characteristic spectra of fragmentation (Versteegh et al., 1997). The LDI SST was calculated following the calibration of de Bar et al. (2020), based on globally distributed marine surface sediments and covers a temperature range from −1.8 to 30.3°C with a calibration error of 3°C

$$\text{with } LDI = [C_{30}1,15-diol]/([C_{28}1,13-diol] + [C_{30}1,13-diol] + [C_{30}1,15-diol]) \tag{2}$$

After calculation of the fractional abundances of the C_{28} and C_{30} 1,14-diols, C_{30} 1,15-diol and C_{28} and C_{30} 1,13-diols, the Diol Index (DI) was calculated following Rampen et al. (2008)

$$\text{with } DI = ([C_{28}1,14-diol] + [C_{30}1,14-diol])/([C_{28}1,14-diol] + [C_{30}1,14-diol] + [C_{30}1,15-diol]) \tag{3}$$

The distribution of LCDs in core NIOP905 has been reported before (Rampen et al., 2008), but LCDs were re-analyzed here using an improved GC-MS method (de Bar et al., 2017). Comparisons showed that our results were similar with the previously published values (Figure S2 in Supporting Information S1).

4. Results

We compiled and generated SST records of cores 74KL and NIOP905 for 0–25 kyr and of cores PASOM3 and 289KL 0–35 kyr (Table 1). Except for core PASOM3, we compiled data from previous studies concerning $U^{K'}_{37}$, and the $\delta^{18}O$ and Mg/Ca ratio of the planktonic foraminiferal species *Globigerinoides ruber*. We applied the same calibrations for all proxies and, therefore, re-calculated the $U^{K'}_{37}$- and $Mg/Ca_{G.ruber}$-derived SSTs (after Müller et al. (1998) and Anand et al. (2003), respectively) for all records. We generated LDI-derived SST records for all cores as well those obtained by $U^{K'}_{37}$, and $\delta^{18}O$ and Mg/Ca ratio data of *G. ruber* from the PASOM3 core. Based on these records, we estimated average SSTs for the Last Glacial Maximum (LGM; 19–22 kyr) and the late Holocene (0–5 kyr for NIOP905 and 74KL; 3–5 kyr for PASOM3, and 2–5 kyr for 289KL) and calculated an approximate SST change ΔSST (LGM-late Holocene) (Table 2). The downcore Mg/Ca ratio-based SST estimations of core 74KL are limited to four discrete specific time intervals (Dahl & Oppo, 2006).

The PASOM3 *G. ruber* oxygen isotopic record ($\delta^{18}O_{G.ruber}$) showed changes coinciding with the glacial-interglacial transition with positive values during the glacial and negative values during the Holocene (Figure 2a). The $Mg/Ca_{G.ruber}$ SST in PASOM3 showed fluctuations between 22 and 27°C, showing substantial differences within relatively short time intervals, particularly during the Glacial, while the Holocene SSTs were relatively stable at this core location. The LGM–late Holocene difference (ΔSST) was 1.2°C at PASOM3 core (Table 2).

The $U^{K'}_{37}$ SST estimations of PASOM3 showed substantial fluctuations throughout the record. The SSTs during 29–35 kyr BP period were slightly lower than present day whereas during the following period SSTs were variable
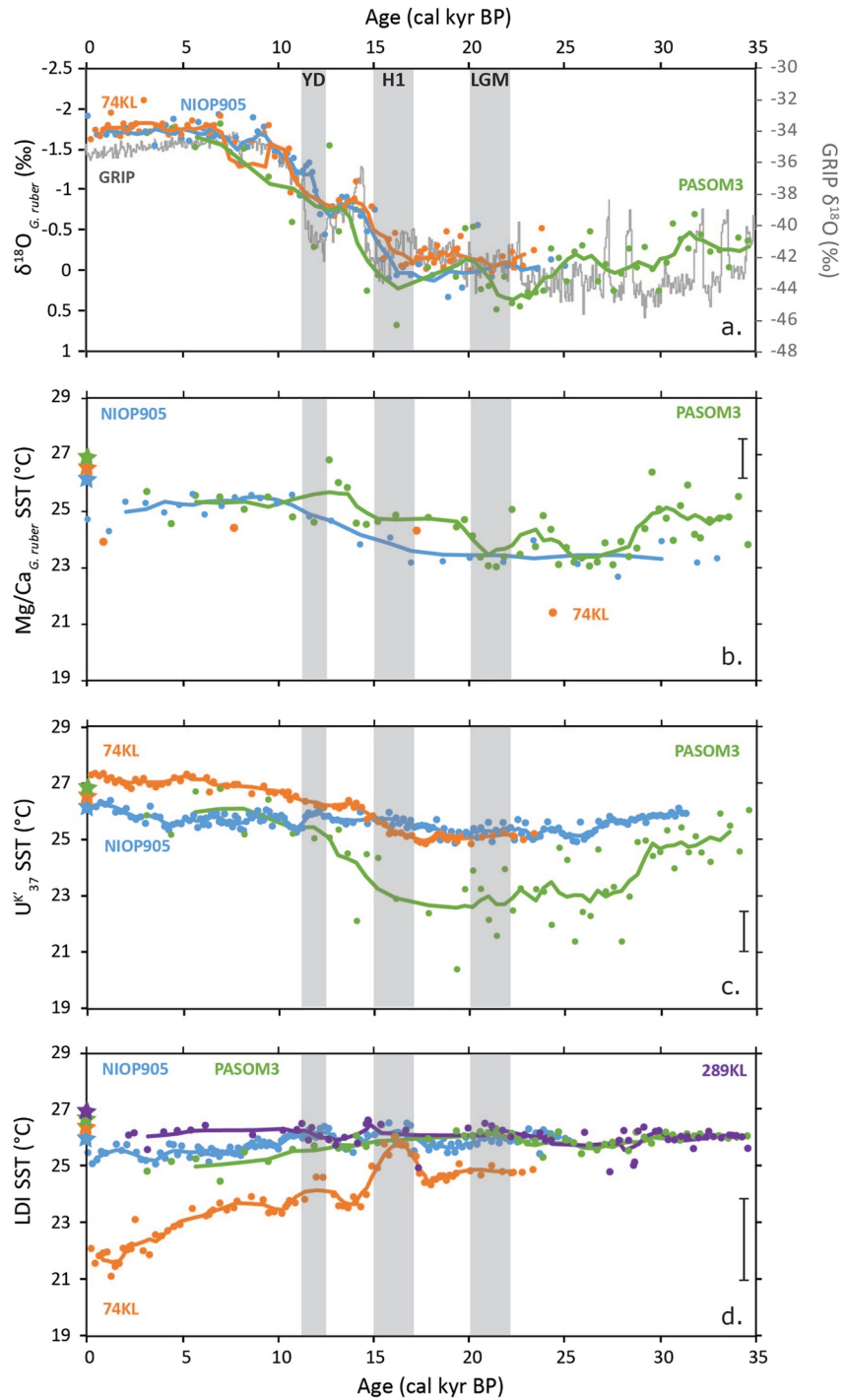
Figure 2. Sea surface temperature (SST) proxy records (b)–(d) for four Arabian Sea sediment cores together with oxygen isotope records of *G. ruber* ($\delta^{18}O_{G.ruber}$) and, for reference, the Greenland ice core (GRIP; $\delta^{18}O$) (a); see Table 1. Calibration errors for each proxy (Mg/Ca: 1.5°C, $U^{K'}_{37}$: 1.5°C, LDI: 3°C) are indicated as bars in each graph. Thick lines show the 5-point moving average. The late Holocene (0–5 kyr BP) of core PASOM3 is not well represented due to low sedimentation rates during this period and loss of the core top (first available data point is, therefore, from 3 kyr BP). The present-day mean annual SST in the Arabian Sea for each core site, based on WOA13 database (Locarnini et al., 2013) is indicated with stars on each scale bar. Specific periods are indicated by gray shaded bars: that is, Younger Dryas (YD), Heinrich Stadial 1 (H1), and LGM: Last Glacial Maximum.

with minimum temperatures of 20.4°C during the LGM. The maximum estimated SST was 26.8°C during the Holocene (Figure 2c). The LGM-late Holocene $U^{K'}_{37}$ SST difference was 3.4°C (Table 2). This SST record showed continuous warming during the deglaciation and Holocene with interruptions during the Heinrich Stadial 1 (H1) and the Younger Dryas (YD; Figure 2c). The $U^{K'}_{37}$-derived SST for the core top (ca. 3.1 kyr BP) was 25.8°C.

The LDI SST records of the northern cores, PASOM3 and 289KL, did not reveal major fluctuations during the last 35 kyr, with minimum temperatures of 24.4°C and 24.8°C and maximum temperatures of 26.3°C and 26.6°C, respectively (Figure 2d). The LDI SST records from the cores in the western Arabian Sea, NIOP905 and 74KL, covering the last 25 kyr indicated fluctuating SSTs from the LGM (19–22 kyr BP) and onwards with minimum SSTs of 25°C and 21°C, and maximum SSTs of 27°C and 26°C, respectively. NIOP905 LDI SSTs indicated minimal changes over this period (−0.5°C). Overall, all LDI-derived SST records of NIOP905, 289KL and PASOM3 showed a small decreasing trend from H1 to the late Holocene, with a major change observed at core 74KL. The difference in LDI SSTs from the LGM to the late Holocene (0–5 cal kyr BP) was observed to be −1.6°C at PA-SOM3, −0.2°C at 289KL, −0.8°C at NIOP905, and −2.7°C at 74KL, respectively (Table 2). All cores revealed higher reconstructed SSTs during the H1 and YD with the largest changes observed at 74KL. Core top (0 kyr BP for NIOP905 and 74KL) LDI-derived SSTs in the western cores were 25.4°C and 22.1°C, respectively, whereas those in the northern cores (ca. 3.1 kyr BP for PASOM3 and ca. 2.2 kyr BP for 289KL) were 24.7°C and 26.1°C, respectively.

5. Discussion

5.1. Arabian Sea Temperature Records Using Established Proxies

Our newly generated PASOM3 $\delta^{18}O_{G.ruber}$ record is similar to other $\delta^{18}O_{G.ruber}$ Arabian Sea records and they all show agreement with the Greenland ice core $\delta^{18}O$ trend (Johnsen et al., 2001), indicating that these records reflect -the northern hemisphere climate dynamics (Figure 2). The Mg/Ca ratio-derived SST record from the PASOM3 core shows a larger variability than that of NIOP905 but shows a similar trend from LGM to late Holocene with an approximately 1–2°C warming (Table 2). This is somewhat smaller than the 2.5°C warming reported for the 74KL record (Dahl & Oppo, 2006, Table 2), but it should be noted that that was only determined by a single data point in the LGM. During the Holocene Mg/Ca ratio-derived SSTs of NIOP905 and PASOM3 follow a relatively stable trend with only slight cooling during the late Holocene. Considering the present day mean annual SST of the Arabian Sea (26–27°C; Locarnini et al., 2013) and the calibration error of Mg/Ca$_{G.ruber}$ (ca. 1.5°C; Anand et al., 2003) Mg/Ca ratio-derived SST estimates of 24–25°C from core tops of the western cores (NIOP905 and 74KL) are somewhat low. Based on observations on the modern specimens of *G. ruber* and the Mg/Ca-based SST calibrations in the Arabian Sea (Conan & Brummer, 2000; Curry et al., 1992), SST estimates were observed to be 1.7 ± 0.8°C lower than annual mean SST (Peeters et al., 2002). This is potentially due to the present-day habitat of *G. ruber* in the Arabian Sea, where this species was observed living year around, calcifying in the uppermost part of the water column and with blooms during both monsoon seasons in relatively cold surface waters (Curry et al., 1992; Dahl & Oppo, 2006).

The newly obtained $U^{K'}_{37}$-derived SST record of PASOM3 shows a high variability but the five-point running mean shows a similar trend as other previously published $U^{K'}_{37}$-derived SST records and follows the $\delta^{18}O_{G.ruber}$ as well as the global climate trend with lower SST values during the LGM and increasing toward the Holocene (Figure 2). However, $U^{K'}_{37}$-derived SSTs for the LGM were substantially lower in our PASOM3 record from the Northern Arabian Sea compared to other two $U^{K'}_{37}$-derived SST records from the western part and showed a much larger LGM to Holocene change (i.e., 3.4°C; Table 2). This is in accordance with previous observations based on $U^{K'}_{37}$ SSTs from the region Gaye et al. (2018 and references cited therein), which showed a higher overall SST change from the Glacial to the Holocene in the northern Arabian Sea compared to the western part. This observation has been interpreted as a result of much stronger NE monsoon and thus cooled surface waters in the N Arabian Sea during the Glacial (Reichart et al., 2004). Furthermore, the SW monsoon-induced upwelling was reduced or inactive in the western Arabian Sea during the Glacial, resulting in warmer Glacial SSTs in the west compared to the north (e.g., Böll et al., 2015). Lower gradient deglacial SST change in the western Arabian Sea has also been linked to changing monsoon dynamics. As a result of reduced impact of NE monsoon related cooling and/or strengthening SW monsoon induced upwelling in the region after the Glacial (Dahl & Oppo, 2006; Emeis et al., 1995; Gaye et al., 2018; Rostek et al., 1997), the SW monsoon and upwelling in the western Arabian Sea intensified and resulted in cooler SSTs in comparison with the northern Arabian Sea (e.g., Anand et al., 2008;

Böll et al., 2015; Gaye et al., 2018). However, the $U^{K'}_{37}$-derived SST record of NIOP905 shows even cooler surface water conditions during the Holocene in comparison with those of the other western Arabian Sea core 74KL (Figure 2c). This is potentially due to a local feature and circulation pattern observed in the region (Figure 1b; e.g., Sonzogni et al., 1998). Right above the core site, the so-called *Great Whirl* develops and remains stationary during the SW Monsoon, which has a major effect on the local SST and surface productivity (Beal & Donohue, 2013; Fischer et al., 1996; Koning et al., 2001; Peeters et al., 1999). This local feature is potentially reflected in $U^{K'}_{37}$ SSTs from core NIOP905, particularly during the Holocene part of the record.

Overall, the SST records based on these proxies reveal relatively small SST change (1–2°C) from LGM to the Holocene, with the exception of PASOM3 (3.4°C). Besides the above-discussed reasons for specific proxy and core site, this is a well-known observation for SST reconstructions in the tropical regions (e.g., CLIMAP Project, 1981; Mix et al., 2001; Rosell-Melé et al., 2004; Waelbroeck et al., 2009). Basin-wide proxy applications (Dahl & Oppo, 2006; Rosell-Melé et al., 2004; Sonzogni et al., 1998) as well as model simulations (Mix et al., 2001; Otto-Bliesner et al., 2009; Waelbroeck et al., 2009) showed that the Arabian Sea SST warming from the LGM to the late Holocene ranged between 1 and 3.5°C, with higher amplitude in the north. The new Mg/Ca ratio and $U^{K'}_{37}$ results from core PASOM3 are also in line with previous observations and model simulations.

5.2. Arabian Sea Temperature Records Using the LDI

The overall trend observed for the LDI-derived SST records are consistent in three of the four records (i.e., except in the 75KL record) but surprisingly only reveal minor changes from glacial to the Holocene (Figure 2d; Table 2) and a slight cooling trend during the Holocene (except for the 289KL record). The small Holocene to LGM SST change and cooling during the Holocene in the LDI records show similarities to the CLIMAP Project data based on planktonic foraminifera SST approaches (modern analogue technique and transfer function), which revealed relatively low LGM-Holocene warming or even cooling at sites in the Arabian Sea between 10 and 20°N interval (CLIMAP Project, 1981; Sonzogni et al., 1998). The LDI record of core 74KL is clearly an exception to the other three (Figure 2d) in that it shows 1.5°C lower glacial SSTs prior to Heinrich Stadial 1 (H1) as well as a strong continuous decline in SST during the Holocene, arriving at SSTs of ca. 22°C in the upper Holocene. This clearly contrasts most other proxy records discussed above, which shows some degree of LGM to Holocene warming and is incompatible with the global climate trend (Figure 2; Table 2). Most of the differences between LDI and $U^{K'}_{37}$ are generally less than 3°C, that is, within calibration errors, suggesting similar SST estimates, with the clear exception of the last Glacial for PASOM3 and 74KL. However, these absolute differences do not detract from the clear observation that LDI has distinct trends in particular with lower Holocene values compared to the LGM. Interestingly, SSTs estimated from planktonic foraminifera-based transfer functions for core 74KL (Schulz, 1995a, 1995b) also show decreasing values for the Holocene and suggest cooler summer (SW monsoon) SSTs after the H1 although cooling in the LDI is more extreme. In this way, transfer function based SSTs are partly in agreement with the LDI-derived SST trend in the Holocene (Figure 3a). The decreasing trend of LDI SST observed in most of our records during the Holocene may be a direct effect on SST due to intensified upwelling (e.g., Gaye et al., 2018; Marcantonio et al., 2001; Rampen et al., 2008; Sirocko et al., 1996) leading to a summer monsoon (i.e., cold) bias in LDI SSTs. Therefore, the LDI is potentially reflecting SW summer monsoon SSTs rather than annual mean temperatures in the Arabian Sea, particularly after the H1 event. Indeed, the deglacial decrease in LDI-based SSTs is lowest at core site 289KL (−0.2°C; Table 2), which is also the furthest from the modern upwelling cell (Figure 1). Nevertheless, we cannot exclude that other factors not related to SST have impacted the LDI.

Sedimentary oxic degradation has been shown to impact LDI values in Arabian Sea surface sediments due to different degradation rates of 1,13- and 1,15-diols leading to ca. 1.5–2.5°C cooler LDI-reconstructed SSTs in sediments deposited below the OMZ (Rodrigo-Gámiz et al., 2016). Enhanced bottom water ventilation and a weaker OMZ have been inferred for cold periods (e.g., Böning & Bard, 2009; Pichevin et al., 2007; Reichart et al., 1997; Reichart et al., 1998; Schulte et al., 1999), presumably leading to enhanced oxygen exposure times (OETs). The bulk sedimentary $\delta^{15}N$ values from western cores suggest that they experienced weaker denitrification, and thus, the OMZ strength was substantially reduced during these periods (Figure 4). This may have led to lower LDI SST estimates during these colder times for the cores obtained from stations located within the present-day OMZ (NIOP905, PASOM3 and 289KL; Figure 1). In contrast, our results actually indicate relatively warmer conditions, particularly during YD and H1, and cooler SSTs during the Holocene (Figure 2). This suggests that the oxic
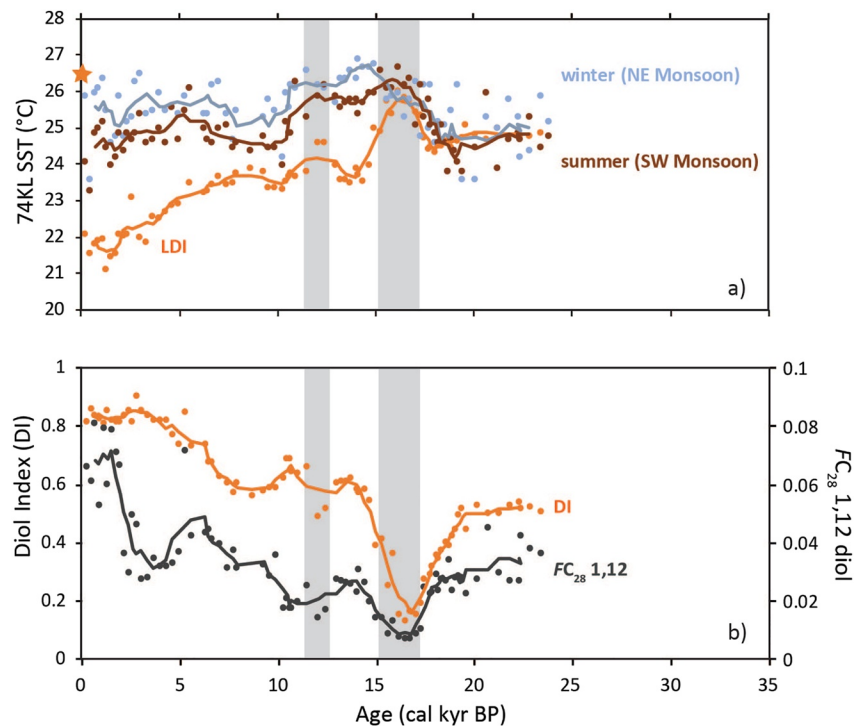
Figure 3. Compilation of various records from core 74KL; (a) SST reconstructions based on LDI and planktonic foraminifera transfer functions for different seasons (light blue: winter, NE monsoon; brown: summer, SW monsoon (Schulz, 1995b), (b) Diol upwelling index (DI) and C_{28} 1,12-diol factor showing potential influence of diatom productivity on the LDI. Largest convergence between the LDI and the planktonic foraminifera transfer function SSTs coincide with periods characterized by reduced upwelling. LDI SSTs show continuous decrease where DI and 1,12-diol increase. Star on the *Y*-axis shows the present annual mean SST at the core site based on World Ocean Atlas13 (Locarnini et al., 2013).

degradation of the LCDs likely did not significantly affect these LDI records. Being by far the deepest core site, 74KL has always been below the OMZ (Figure 1), and the sediments deposited probably have been impacted by much longer oxygen exposure times (OET) than the other sedimentary records studied. These enhanced OET may have led to an overall cold bias compared to other cores, especially during the Holocene when other sites may have been within the OMZ and therefore experienced lower OET (Figure 2d).

A cold bias in SSTs reconstructed with the LDI could also occur when groups of organisms, such as *Proboscia* diatoms, produce, in addition to their characteristic 1,14-diols, also 1,13- and 1,15-diols as has been observed around Iceland (Rodrigo-Gámiz et al., 2015). de Bar et al. (2020) reported that such a bias in LDI could be assessed by the relative abundance of 1,12-diols, produced by certain *Proboscia* diatoms, expressed in the FC_{28} 1,12. However, in all of our records, FC_{28} 1,12 remained well below the threshold (<0.1), with values below 0.02 in most of the records (Figure S3 in Supporting Information S1). Only, Holocene values at core 74KL were getting close to the threshold of 0.1 (Figure 3). Nevertheless, the Diol Index (DI), a proxy for upwelling intensity and enhanced nutrient concentrations, does show increasing values in all sites after the last deglaciation (Figures 3 and 4), as previously reported for core NIOP905 (Rampen et al., 2008), suggesting an overall increase in *Proboscia* diatom contributions. However, except for core 74KL, the LDI SST estimates during the Holocene fit well with other temperature proxies as well as modern day SST (Figures 2 and 3), despite having relatively high DI values. Hence, these changes in upwelling and concomitantly increasing nutrient availability cannot explain the relatively high LDI-reconstructed SSTs during the glacial.

As discussed, LDI-reconstructed SSTs for core 74KL remain very unusual compared to the other cores as they show the highest SSTs during cold intervals, the YD and H1, and a continuously decreasing trend during the Holocene with the largest offset from the LGM to the Holocene (ΔSST = −2.7°C; Table 2). This is also quite different from a previously published TEX86 temperature record from the same core (Huguet et al., 2006a; Figure S4 in Supporting Information S1), suggesting something affected the LDI in particular during the Holocene. Core
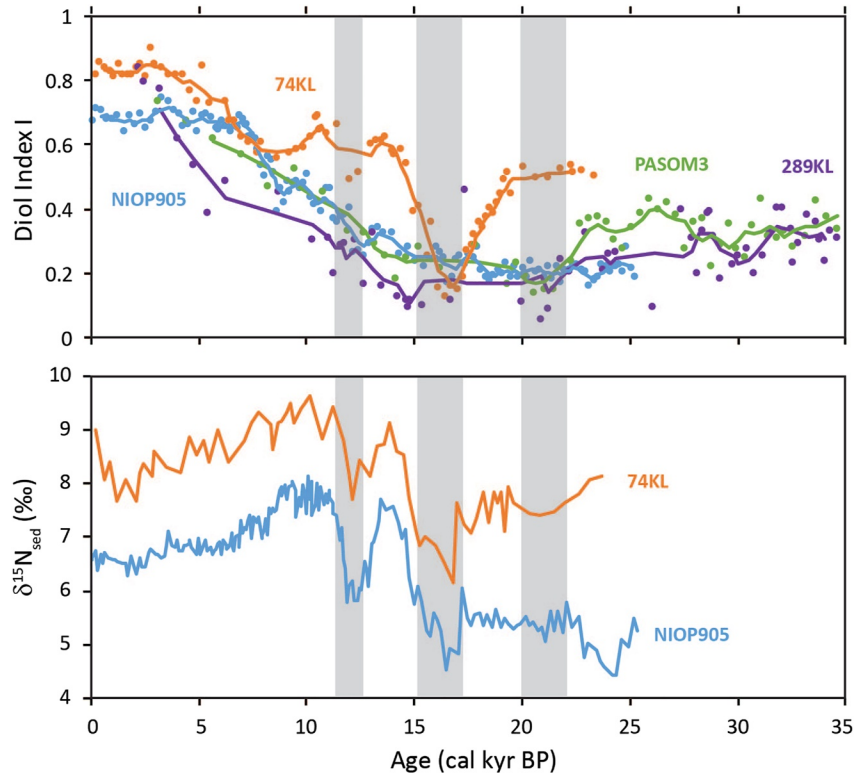
Figure 4. Records for the Diol upwelling index (DI) for the four stations considered in this study and bulk sedimentary $\delta^{15}N$ from western sites, 74KL and NIOP 905 [data from Suthhof et al. (2001) and Ivanochko et al. (2005), respectively].

74KL was collected in an area where the SW monsoon and related upwelling are much more pronounced today in comparison to the northern part of the Arabian Sea. Indeed, we observe strong correlation between the DI and LDI ($r2 = 0.72$) at core 74KL. This is intriguing as we do not see a similar trend in core NIOP905 despite the similar upwelling dynamics. However, the OMZ is much stronger within the overlying waters of the 74KL core site, in comparison to the other western core NIOP905 (Figure 1; Garcia et al., 2013). This also has been the case during the past 25 kyr as indicated by the $\delta^{15}N_{sed}$ values (>6‰ at core 74KL; Figure 4). Overall, the $\delta^{15}N_{sed}$ show similar trends at both cores with lower values at NIOP905 in comparison to 74KL. Both cores also show similar trends with the DI until the onset of the Holocene, particularly at core 74KL, suggesting a close link between upwelling conditions and nutrient dynamics. The link between climate variability, nutrient, and OMZ dynamics in the region is well-documented (e.g., Altabet et al., 2002). These local differences and available information suggest that the extent of the OMZ in combination with enhanced upwelling might have a pronounced impact on the LDI and LCD producers at the 74KL location, which needs further investigation.

6. Conclusions

A multi proxy application in series of cores from the western and northeastern part of the Arabian Sea emphasizes the importance of application of different proxies and on several records to reconstruct regional climate dynamics. Our results show that LDI is likely to reflect in part summer monsoonal temperatures showing little change in SST from glacial to the Holocene and is not an ideally suited proxy to reconstruct annual mean SST in the Arabian Sea. The index may also be potentially biased by upwelling intensity and related nutrient input in regions of strong upwelling and extended OMZs. Results from LDI in upwelling regions should therefore be interpreted carefully. However, other SST proxies such as $U^{K'}_{37}$ and $Mg/Ca_{G.ruber}$ show also variable trends though they mostly document a relatively consistent overall SST increase from the Last Glacial Maximum (LGM) to the late Holocene of 1–2°C, with a larger amplitude in the northern Arabian Sea in comparison with the west.

Data Availability Statement

Datasets for this research are available in these in-text data citation references: Schulz, H. (1995): https://doi.pangaea.de/10.1594/PANGAEA.134165, Huguet et al. (2006b, 2006c): https://doi.org/10.1594/PANGAEA.861247 and https://doi.org/10.1594/PANGAEA.861245, Dahl and Oppo (2006): https://doi.org/10.1594/PANGAEA.834987. The new data presented in this study can be reached through following links: https://doi.pangaea.de/10.1594/PANGAEA.931940; https://doi.org/10.4121/17013755.v1 and https://doi.org/10.4121/17014052.v1. All data used for this study is with the license Creative Commons Attribution 4.0 International (CC-BY-4.0).

References

Acharya, S. S., & Panigrahi, M. K. (2016). Eastward shift and maintenance of Arabian Sea oxygen minimum zone: Understanding the paradox. *Deep Sea Research Part I: Oceanographic Research Papers*, *115*, 240–252. https://doi.org/10.1016/j.dsr.2016.07.004

Altabet, M. A., Higginson, M. J., & Murray, D. W. (2002). The effect of millennial-scale changes in Arabian Sea denitrification on atmospheric CO_2. *Nature*, *415*, 159–162. https://doi.org/10.1038/415159a

Anand, P., Elderfield, H., & Conte, M. H. (2003). Calibration of Mg/Ca thermometry in planktonic foraminifera from a sediment trap time series. *Paleoceanography*, *18*(2). https://doi.org/10.1029/2002pa000846

Anand, P., Kroon, D., Singh, A. D., Ganeshram, R. S., Ganssen, G., & Elderfield, H. (2008). Coupled sea surface temperature-seawater δ18O reconstructions in the Arabian Sea at the millennial scale for the last 35 ka. *Paleoceanography*, *23*(4). https://doi.org/10.1029/2007pa001564

Andersen, K. K., Azuma, N., Barnola, J.-M., Bigler, M., Biscaye, P., Caillon, N., et al. (2004). High-resolution record of Northern Hemisphere climate extending into the last interglacial period. *Nature*, *431*(7005), 147–151.

Balzano, S., Lattaud, J., Villanueva, L., Rampen, S. W., Brussaard, C. P., Van Bleijswijk, J., et al. (2018). A quest for the biological sources of long chain alkyl diols in the western tropical North Atlantic Ocean. *Biogeosciences*, *15*(19), 5951–5968. https://doi.org/10.5194/bg-15-5951-2018

Barker, S., Greaves, M., & Elderfield, H. (2003). A study of cleaning procedures used for foraminiferal Mg/Ca paleothermometry. *Geochemistry, Geophysics, Geosystems*, *4*(9). https://doi.org/10.1029/2003gc000559

Beal, L. M., & Donohue, K. A. (2013). The Great Whirl: Observations of IST seasonal development and interannual variability. *Journal of Geophysical Research: Oceans*, *118*, 1–13. https://doi.org/10.1029/2012JC008198

Böll, A., Schulz, H., Munz, P., Rixen, T., Gaye, B., & Emeis, K.-C. (2015). Contrasting sea surface temperature of summer and winter monsoon variability in the northern Arabian Sea over the last 25 ka. *Palaeogeography, Palaeoclimatology, Palaeoecology*, *426*, 10–21.

Böning, P., & Bard, E. (2009). Millennial/centennial-scale thermocline ventilation changes in the Indian Ocean as reflected by aragonite preservation and geochemical variations in Arabian Sea sediments. *Geochimica et Cosmochimica Acta*, *73*(22), 6771–6788.

Brassell, S. C., Eglinton, G., Marlowe, I. T., Pflaumann, U., & Sarnthein, M. (1986). Molecular stratigraphy: A new tool for climatic assessment. *Nature*, *320*(6058), 129–133. https://doi.org/10.1038/320129a0

Clemens, S. C., & Prell, W. L. (2003). A 350,000 year summer-monsoon multi-proxy stack from the Owen ridge, Northern Arabian sea. *Marine Geology*, *201*(1–3), 35–51. https://doi.org/10.1016/s0025-3227(03)00207-x

CLIMAP Project. (1981). *Seasonal reconstructions of the Earth's surface at the last glacial maximum*. Geological Society of America.

Conan, S. M.-H., & Brummer, G.-J. A. (2000). Fluxes of planktic foraminifera in response to monsoonal upwelling on the Somalia Basin margin. *Deep-Sea Research Part Ii-Topical Studies in Oceanography*, *47*(9–11), 2207–2227. https://doi.org/10.1016/s0967-0645(00)00022-9

Curry, W. B., Ostermann, D. R., Guptha, M. V. S., & Ittekkot, V. (1992). Foraminiferal production and monsoonal upwelling in the Arabian Sea: Evidence from sediment traps. In C. P. Summerhayes, W. L. Prell, & K. C. Emeis (Eds.), *Upwelling Systems: Evolution Since the Early Miocene* (Vol. 64, pp. 93–106). The Geological Society, Special Publications. https://doi.org/10.1144/gsl.sp.1992.064.01.06

Dahl, K. A., & Oppo, D. W. (2006). Sea surface temperature pattern reconstructions in the Arabian Sea. *Paleoceanography*, *21*(1), PA1014. https://doi.org/10.1029/2005pa001162

Dahl, K. A., & Oppo, D. W. (2006). Mg/Ca ratios of Globigerinoides ruber from Arabian Sea sediments. *PANGAEA*. https://doi.org/10.1594/PANGAEA.834987

Dauner, A. L. L., Mollenhauer, G., Bícego, M. C., de Souza, M. M., Nagai, R. H., Figueira, R. C. L., et al. (2019). Multi-proxy reconstruction of sea surface and subsurface temperatures in the western South Atlantic over the last ∼75 kyr. *Quaternary Science Reviews*, *215*, 22–34. https://doi.org/10.1016/j.quascirev.2019.04.020

de Bar, M. W., Hopmans, E. C., Verweij, M., Dorhout, D. J. C., Damste, J. S. S., & Schouten, S. (2017). Development and comparison of chromatographic methods for the analysis of long chain diols and alkenones in biological materials and sediment. *Journal of Chromatography A*, *1521*, 150–160. https://doi.org/10.1016/j.chroma.2017.09.037

de Bar, M. W., Stolwijk, D. J., McManus, J. F., Sinninghe Damste, J. S., & Schouten, S. (2018). A Late Quaternary climate record based on long-chain diol proxies from the Chilean margin. *Climate of the Past*, *14*, 1783–1803. https://doi.org/10.5194/cp-14-1783-2018

de Bar, M. W., Weiss, G., Rampen, S., Lattaud, J., Bale, N. J., Brummer, G.-J. A., et al. (2020). Global temperature calibration of the Long chain Diol Index in marine surface sediments. *Organic Geochemistry*. https://doi.org/10.1016/j.orggeochem.2020.103983

Deplazes, G., Lückge, A., Peterson, L. C., Timmermann, A., Hamann, Y., Hughen, K. A., et al. (2013). Links between tropical rainfall and North Atlantic climate during the last glacial period. *Nature Geoscience*, *6*(3), 213–217. https://doi.org/10.1038/ngeo1712

Deplazes, G., Lückge, A., Stuut, J.-B. W., Pätzold, J., Kuhlmann, H., Husson, D., et al. (2014). Weakening and strengthening of the Indian monsoon during Heinrich events and Dansgaard-Oeschger oscillations. *Paleoceanography*, *29*(2), 99–114. https://doi.org/10.1002/2013pa002509

Doose-Rolinski, H., Rogalla, U., Scheeder, G., Lückge, A., & von Rad, U. (2001). High-resolution temperature and evaporation changes during the late Holocene in the northeastern Arabian Sea. *Paleoceanography*, *16*(4), 358–367.

Elderfield, H., & Ganssen, G. (2000). Past temperature and δ18O of surface ocean waters inferred from foraminiferal Mg/Ca ratios. *Nature*, *405*(6785), 442–445. https://doi.org/10.1038/35013033

Emeis, K.-C., Anderson, D. M., Doose, H., Kroon, D., & Schulz-Bull, D. (1995). Sea-Surface temperatures and the history of monsoon upwelling in the Northwest Arabian Sea during the last 500,000 years. *Quaternary Research*, *43*(3), 355–361. https://doi.org/10.1006/qres.1995.1041

Erez, J., & Luz, B. (1983). Experimental paleotemperature equation for planktonic-foraminifera. *Geochimica et Cosmochimica Acta*, *47*(6), 1025–1031. https://doi.org/10.1016/0016-7037(83)90232-6

Fischer, J., Schott, F., & Stramma, L. (1996). Currents and transports of the Great Whirl-Socotra Gyre system during the summer monsoon, August 1993. *Journal of Geophysical Research: Oceans*, *101*(C2), 3573–3587. https://doi.org/10.1029/95jc03617

Garcia, H. E., Boyer, T. P., Locarnini, R. A., Antonov, J. I., Mishonov, A. V., Baranova, O. K., et al. (2013). *World ocean atlas 2013. Volume 3, Dissolved oxygen, apparent oxygen utilization, and oxygen saturation.*

Gaye, B., Böll, A., Segschneider, J., Burdanowitz, N., Emeis, K.-C., Ramaswamy, V., et al. (2018). Glacial–interglacial changes and Holocene variations in Arabian Sea denitrification. *Biogeosciences*, *15*(2), 507–527. https://doi.org/10.5194/bg-15-507-2018

Gaye-Haake, B., Lahajnar, N., Emeis, K.-C., Unger, D., Rixen, T., Suthhof, A., et al. (2005). Stable nitrogen isotopic ratios of sinking particles and sediments from the northern Indian Ocean. *Marine Chemistry*, *96*(3–4), 243–255. https://doi.org/10.1016/j.marchem.2005.02.001

Haake, B., Ittekkot, V., Rixen, T., Ramaswamy, V., Nair, R. R., & Curry, W. B. (1993). Seasonality and interannual variability of particle fluxes to the deep Arabian Sea. *Deep-Sea Research I*, *40*(7), 1323–1344. https://doi.org/10.1016/0967-0637(93)90114-i

Häggi, C., Schefuß, E., Sawakuchi, A. O., Chiessi, C. M., Mulitza, S., Bertassoli, D. J., et al. (2019). Modern and late Pleistocene particulate organic carbon transport by the Amazon River: Insights from long-chain alkyl diols. *Geochimica et Cosmochimica Acta*, *262*, 1–19. https://doi.org/10.1016/j.gca.2019.07.018

Helly, J. J., & Levin, L. A. (2004). Global distribution of naturally occurring marine hypoxia on continental margins. *Deep Sea Research Part I: Oceanographic Research Papers*, *51*(9), 1159–1168. https://doi.org/10.1016/j.dsr.2004.03.009

Honjo, S., Dymond, J., Prell, W., & Ittekkot, V. (1999). Monsoon-controlled export fluxes to the interior of the Arabian Sea. *Deep-Sea Research Part II*, *46*(8–9), 1859–1902. https://doi.org/10.1016/s0967-0645(99)00047-8

Huguet, C., Kim, J.-H., Sinninghe Damsté, J. S., & Schouten, S. (2006a). Reconstruction of sea surface temperature variations in the Arabian Sea over the last 23 kyr using organic proxies (TEX86 and U37$^{K'}$). *Paleoceanography*, *21*(3). https://doi.org/10.1029/2005pa001215

Huguet, C., Kim, J. H., Sinninghe Damsté, J. S., & Schouten, S. (2006b). Sea surface temperature reconstruction for sediment core SO42-74KL. *PANGAEA*. https://doi.org/10.1594/PANGAEA.861247

Huguet, C., Kim, J. H., Sinninghe Damsté, J. S., & Schouten, S. (2006c). Sea surface temperature reconstruction for sediment core NIOP-C2_905_PC. *PANGAEA*. https://doi.org/10.1594/PANGAEA.861245

Imbrie, J., & Kipp, N. G. (1971). A new micropaleontological method for quantitative paleoclimatology: Application to a late Pleistocene Caribbean core. In K. K. Turekian (Ed.), *The late Cenozoic glacial ages* (pp. 71–181). Yale University Press.

Ivanochko, T. S., Ganeshram, R. S., Brummer, G.-J. A., Ganssen, G., Jung, S. J. A., Moreton, S. G., & Kroon, D. (2005). Variations in tropical convection as an amplifier of global climate change at the millennial scale. *Earth and Planetary Science Letters*, *235*(1–2), 302–314. https://doi.org/10.1016/j.epsl.2005.04.002

Ivanova, E. M., Conan, S. M.-H., Peeters, F. J. C., & Troelstra, S. R. (1999). Living *Neogloboquadrina pachyderma* sin and its distribution in the sediments from Oman and Somalia upwelling areas. *Marine Micropaleontology*, *36*(2–3), 91–107. https://doi.org/10.1016/s0377-8398(98)00027-9

Johnsen, S. J., Dahl-Jensen, D., Gundestrup, N., Steffensen, J. P., Clausen, H. B., Miller, H., et al. (2001). Oxygen isotope and palaeotemperature records from six Greenland ice-core stations: Camp Century, Dye-3, GRIP, GISP2, Renland and NorthGRIP. *Journal of Quaternary Science: Published for the Quaternary Research Association*, *16*(4), 299–307. https://doi.org/10.1002/jqs.622

Johnstone, H. J. H., Steinke, S., Kuhnert, H., Bickert, T., PälikeMohtadi, M., & Mohtadi, M. (2016). Automated cleaning of foraminifera shells before Mg/Ca analysis using a pipette robot. *Geochemistry, Geophysics, Geosystems*, *17*, 3502–3511. https://doi.org/10.1002/2016GC006422

Jonas, A. S., Schwark, L., & Bauersachs, T. (2017). Late Quaternary water temperature variations of the Northwest Pacific based on the lipid paleothermometers TEX H 86, U K´ 37 and LDI. *Deep Sea Research Part I: Oceanographic Research Papers*, *125*, 81–93. https://doi.org/10.1016/j.dsr.2017.04.018

Jung, S. J. A., Davies, G. R., Ganssen, G., & Kroon, D. (2002). Decadal-centennial scale monsoon variations in the Arabian Sea during the Early Holocene. *Geochemistry, Geophysics, Geosystems*, *3*. https://doi.org/10.1029/2002gc000348

Jung, S. J. A., Ganssen, G., & Davies, G. R. (2001). Multidecadal variation in the early Holocene outflow or Red Sea Water into the Arabian Sea. *Paleoceanography*, *16*(6), 658–668. https://doi.org/10.1029/2000pa000592

Kim, J.-H., Rimbu, N., Lorenz, S. J., Lohmann, G., Nam, S. I., Schouten, S., & Schneider, R. R. (2004). North Pacific and North Atlantic sea-surface temperature variability during the Holocene. *Quaternary Science Reviews*, *23*(20–22), 2141–2154. https://doi.org/10.1016/j.quascirev.2004.08.010

Koning, E., van Iperen, J. M., van Raaphorst, W., Helder, W., Brummer, G.-J. A., & van Weering, T. C. E. (2001). Selective preservation of upwelling-indicating diatoms in sediments off Somalia, NW Indian Ocean. *Deep-Sea Research I*, *48*, 2473–2495. https://doi.org/10.1016/s0967-0637(01)00019-x

Kucera, M., Rosell-Melé, A., Schneider, R., Waelbroeck, C., & Weinelt, M. (2005). Multiproxy approach for the reconstruction of the glacial ocean surface (MARGO). *Quaternary Science Reviews*, *24*(7–9), 813–819. https://doi.org/10.1016/j.quascirev.2004.07.017

Lattaud, J., Lo, L., Huang, J. J., Chou, Y. M., Gorbarenko, S. A., Sinninghe Damsté, J. S., & Schouten, S. (2018). A comparison of late quaternary organic proxy-based paleotemperature records of the Central Sea of Okhotsk. *Paleoceanography and Paleoclimatology*. https://doi.org/10.1029/2018pa003388

Lear, C. H., Coxall, H. K., Foster, G. L., Lunt, D. J., Mawbey, E. M., Rosenthal, Y., et al. (2015). Neogene ice volume and ocean temperatures: Insights from infaunal foraminiferal Mg/Ca paleothermometry. *Paleoceanography*, *30*, 1437–1454. https://doi.org/10.1002/2015PA002833

Locarnini, R. A., Mishonov, A. V., Antonov, J. I., Boyer, T. P., Garcia, H. E., Baranova, O. K., et al. (2013). World Ocean Atlas 2013 Volume 1: Temperature. In S. Levitus, & A. Mishonov (Eds.), *NOAA Atlas NESDIS 73* (Vol. 73, p. 40).

Lopes dos Santos, R. A., Spooner, M. I., Barrows, T. T., De Deckker, P., Sinninghe Damsté, J. S., & Schouten, S. (2013). Comparison of organic (U^{K37}, TEX^{H86}, LDI) and faunal proxies (foraminiferal assemblages) for reconstruction of late Quaternary sea surface temperature variability from offshore southeastern Australia. *Paleoceanography*, *28*, 377–387. https://doi.org/10.1002/palo.20035

Marcantonio, F., Anderson, R. F., Higgins, S., Fleisher, M. Q., Stute, M., & Schlosser, P. (2001). Abrupt intensification of the SW Indian Ocean monsoon during the last deglaciation: Constraints from Th, Pa, and He isotopes. *Earth and Planetary Science Letters*, *184*(2), 505–514. https://doi.org/10.1016/s0012-821x(00)00342-3

Mezger, E. M. (2019). *Controls on sodium incorporation in foraminiferal calcite. Utrecht Studies in Earth Sciences* (PhD Thesis) (Vol. 182, p. 241). Utrecht University. Retrieved from https://hdl.handle.net/1874/380001

Mezger, E., Nooijer, L., Boer, W., Brummer, G., & Reichart, G. (2016). Salinity controls on Na incorporation in Red Sea planktonic foraminifera. *Paleoceanography and Paleoclimatology*, *31*(12), 1562–1582. https://doi.org/10.1002/2016pa003052

Mix, A. C., Bard, E., & Schneider, R. (2001). Environmental processes of the ice age: Land, oceans, glaciers (EPILOG). *Quaternary Science Reviews*, *20*(4), 627–657. https://doi.org/10.1016/s0277-3791(00)00145-1

Müller, P. J., Kirst, G., Ruhland, G., von Storch, I., & Rosell-Melé, A. (1998). Calibration of the alkenone paleotemperature index U$^{K'}_{37}$ based on core-tops from the eastern South Atlantic and the global ocean (60°N-60°S). *Geochimica et Cosmochimica Acta*, *62*(10), 1757–1772.

Naqvi, W. A. (1991). Geographical extent of denitrification in the Arabian Sea in relation to some physical processes. *Oceanologica Acta*, *14*(3), 281–290.

Nürnberg, D., Bijma, J., & Hemleben, C. (1996). Assessing the reliability of magnesium in foraminiferal calcite as a proxy for water mass temperatures. *Geochimica et Cosmochimica Acta*, *60*(5), 803–814.

Okai, T., Suzuki, A., Kawahata, H., Terashima, S., & Imai, N. (2002). Preparation of a new Geological Survey of Japan geochemical reference material: Coral JCp-1. *Geostandards Newsletter*, *26*(1), 95–99. https://doi.org/10.1111/j.1751-908x.2002.tb00627.x

Olson, D. B., Hitchcock, G. L., Fine, R. A., & Warren, B. A. (1993). Maintenance of the low-oxygen layer in the central Arabian Sea. *Deep-Sea Research Part Ii-Topical Studies in Oceanography*, *40*(3), 673–685. https://doi.org/10.1016/0967-0645(93)90051-n

Otto-Bliesner, B. L., Schneider, R., Brady, E., Kucera, M., Abe-Ouchi, A., Bard, E., et al. (2009). A comparison of PMIP2 model simulations and the MARGO proxy reconstruction for tropical sea surface temperatures at last glacial maximum. *Climate Dynamics*, *32*(6), 799–815. https://doi.org/10.1007/s00382-008-0509-0

Paulmier, A., & Ruiz-Pino, D. (2009). Oxygen minimum zones (OMZs) in the modern ocean. *Progress in Oceanography*, *80*(3–4), 113–128. https://doi.org/10.1016/j.pocean.2008.08.001

Peeters, F., Brummer, G.-J., Ganssen, G. (2002). The effect of upwelling on the distribution and stable isotope composition of Globigerina bulloides and Globigerinoides ruber (planktic foraminifera) in modern surface waters of the NW Arabian Sea. *Global and Planetary Change*, *34*(3–4), 269–291.

Peeters, F., Ivanova, E., Conan, S., Brummer, G.-J., Ganssen, G., Troelstra, S., & van Hinte, J. (1999). A size analysis of planktic foraminifera from the Arabian Sea. *Marine Micropaleontology*, *36*(1), 31–63. https://doi.org/10.1016/s0377-8398(98)00026-7

Pflaumann, U., Duprat, J., Pujol, C., & Labeyrie, L. D. (1996). SIMMAX: A modern analog technique to deduce Atlantic sea surface temperatures from planktonic foraminifera in deep-sea sediments. *Paleoceanography*, *11*(1), 15–35. https://doi.org/10.1029/95pa01743

Pichevin, L., Bard, E., Martinez, P., & Billy, I. (2007). Evidence of ventilation changes in the Arabian Sea during the late Quaternary: Implication for denitrification and nitrous oxide emission. *Global Biogeochemical Cycles*, *21*(4). https://doi.org/10.1029/2006gb002852

Prahl, F. G., & Wakeham, S. G. (1987). Calibration of unsaturation patterns in long-chain ketone compositions for palaeotemperature assessment. *Nature*, *330*, 367–369. https://doi.org/10.1038/330367a0

Prasad, T., Ikeda, M., & Kumar, S. P. (2001). Seasonal spreading of the Persian Gulf Water mass in the Arabian Sea. *Journal of Geophysical Research: Oceans*, *106*(C8), 17059–17071. https://doi.org/10.1029/2000jc000480

Qasim, S. Z. (1982). Oceanography of the Northern Arabian Sea. *Deep-Sea Research Part A-Oceanographic Research Papers*, *29*(9A), 1041–1068. https://doi.org/10.1016/0198-0149(82)90027-9

Rampen, S. W., Schouten, S., Koning, E., Brummer, G.-J. A., & Damsté, J. S. S. (2008). A 90 kyr upwelling record from the northwestern Indian Ocean using a novel long-chain diol index. *Earth and Planetary Science Letters*, *276*(1), 207–213. https://doi.org/10.1016/j.epsl.2008.09.022

Rampen, S. W., Willmott, V., Kim, J.-H., Rodrigo-Gámiz, M., Uliana, E., Mollenhauer, G., et al. (2014). Evaluation of long chain 1, 14-alkyl diols in marine sediments as indicators for upwelling and temperature. *Organic Geochemistry*, *76*, 39–47. https://doi.org/10.1016/j.orggeochem.2014.07.012

Rampen, S. W., Willmott, V., Kim, J.-H., Uliana, E., Mollenhauer, G., Schefuß, E., et al. (2012). Long chain 1, 13-and 1, 15-diols as a potential proxy for palaeotemperature reconstruction. *Geochimica et Cosmochimica Acta*, *84*, 204–216. https://doi.org/10.1016/j.gca.2012.01.024

Reichart, G. J., Brinkhuis, H., Huiskamp, F., & Zachariasse, W. J. (2004). Hyperstratification following glacial overturning events in the northern Arabian Sea. *Paleoceanography*, *19*(2). https://doi.org/10.1029/2003pa000900

Reichart, G. J., den Dulk, M., Visser, H. J., van der Weijden, C. H., & Zachariasse, W. J. (1997). A 225 kyr record of dust supply, paleoproductivity and the oxygen minimum zone from the Murray ridge (northern Arabian sea). *Palaeogeography, Palaeoclimatology, Palaeoecology*, *134*(1–4), 149–169. https://doi.org/10.1016/s0031-0182(97)00071-0

Reichart, G. J., Lourens, L. J., & Zachariasse, W. J. (1998). Temporal variability in the northern Arabian Sea Oxygen Minimum Zone (OMZ) during the last 225,000 years. *Paleoceanography*, *13*(6), 607–621. https://doi.org/10.1029/98pa02203

Reichart, G. J., Nortier, J., Versteegh, G., & Zachariasse, W. J. (2002a). Periodical breakdown of the Arabian Sea oxygen minimum zone caused by deep convective mixing. In P. D. Clift, D. Kroon, C. Gaedicke, & J. Craig (Eds.), *The tectonic and climatic evolution of the Arabian Sea region* (Vol. 195, pp. 407–419). The Geological Society, London, Special Publications. https://doi.org/10.1144/gsl.sp.2002.195.01.22

Reichart, G. J., Schenau, S. J., De Lange, G. J., & Zachariasse, W. J. (2002b). Synchroneity of oxygen minimum zone intensity on the Oman and Pakistan Margins at sub-Milankovitch time scales. *Marine Geology*, *185*(3–4), 403–415. https://doi.org/10.1016/s0025-3227(02)00184-6

Reimer, P. J., Bard, E., Bayliss, A., Beck, J. W., Blackwell, P. G., Ramsey, C. B., et al. (2013). IntCal13 and Marine13 radiocarbon age calibration curves 0–50,000 years cal BP. *Radiocarbon*, *55*(4), 1869–1887. https://doi.org/10.2458/azu_js_rc.55.16947

Rixen, T., Baum, A., Gaye, B., & Nagel, B. (2014). Seasonal and interannual variations in the nitrogen cycle in the Arabian Sea. *Biogeosciences*, *11*(20), 5733–5747. https://doi.org/10.5194/bg-11-5733-2014

Rixen, T., Ittekkot, V., Haake-Gaye, B., & Schäfer, P. (2000). The influence of the SW monsoon on the deep-sea organic carbon cycle in the Holocene. *Deep-Sea Research Part Ii-Topical Studies in Oceanography*, *47*(14), 2629–2651. https://doi.org/10.1016/s0967-0645(00)00042-4

Rodrigo-Gámiz, M., Rampen, S. W., de Haas, H., Baas, M., Schouten, S., & Sinninghe Damsté, J. S. (2015). Constraints on the applicability of the organic temperature proxies UK'37, TEX86 and LDI in the subpolar region around Iceland. *Biogeosciences*, *12*(22), 6573–6590. https://doi.org/10.5194/bg-12-6573-2015

Rodrigo-Gámiz, M., Rampen, S. W., Schouten, S., & Sinninghe Damsté, J. S. (2016). The impact of oxic degradation on long chain alkyl diol distributions in Arabian Sea surface sediments. *Organic Geochemistry*, *100*, 1–9. https://doi.org/10.1016/j.orggeochem.2016.07.003

Rosell-Melé, A., Bard, E., Emeis, K.-C., Grieger, B., Hewitt, C., Müller, P. J., & Schneider, R. R. (2004). Sea surface temperature anomalies in the oceans at the LGM estimated from the alkenone-$U^{K'}_{37}$ index: Comparison with GCMs. *Geophysical Research Letters*, *31*(3), L03208-03201–L03208-03204.

Rostek, F., Bard, E., Beaufort, L., Sonzogni, C., & Ganssen, G. (1997). Sea surface temperature and productivity records for the past 240 kyr in the Arabian Sea. *Deep-Sea Research II*, *44*(6–7), 1461–1480. https://doi.org/10.1016/s0967-0645(97)00008-8

Sarma, V. (2002). An evaluation of physical and biogeochemical processes regulating perennial suboxic conditions in the water column of the Arabian Sea. *Global Biogeochemical Cycles*, *16*(4). https://doi.org/10.1029/2001gb001461

Schlitzer, R. (2015). *Ocean data view*. https://odv.awi.de

Schmidt, H., Czeschel, R., & Visbeck, M. (2020). Seasonal variability of the Arabian Sea intermediate circulation and its impact on seasonal changes of the upper oxygen minimum zone. *Ocean Science*, *16*(6), 1459–1474. https://doi.org/10.5194/os-16-1459-2020

Schulte, S., & Müller, P. J. (2001). Variations of sea surface temperature and primary productivity during Heinrich and Dansgaard-Oescher events in the northeastern Arabian Sea. *Geo-Marine Letters*, *21*, 168–175. https://doi.org/10.1007/s003670100080

Schulte, S., Rostek, F., Bard, E., Rullkötter, J., & Marchal, O. (1999). Variations of oxygen-minimum and primary productivity recorded in sediments of the Arabian Sea. *Earth and Planetary Science Letters*, *173*(3), 205–221. https://doi.org/10.1016/s0012-821x(99)00232-0

Schulz, H. (1995a). *Meeresoberflächentemperaturen vor 10.000 Jahren-Auswirkungen des frühholozänen Insolationsmaximums*. Berichte-Reports (Vol. 73, p. 119). Geologisch-Paläontologisches Institut und Museum, Christian-Albrechts-Universität.

Schulz, H. (1995b). *Sea surface temperatures calculated for sediment core SO42-74KL.* https://doi.org/10.1594/PANGAEA.51953

Schulz, H., von Rad, U., Erlenkeuser, H., & von Rad, U. (1998). Correlation between Arabian Sea and Greenland climate oscillations of the past 110,000 years. *Nature*, *393*(6680), 54–57. https://doi.org/10.1038/31750

Shakun, J. D., Clark, P. U., He, F., Marcott, S. A., Mix, A. C., Liu, Z., et al. (2012). Global warming preceded by increasing carbon dioxide concentrations during the last deglaciation. *Nature*, *484*, 49–54. https://doi.org/10.1038/nature10915

Shankar, D., Shenoi, S., Nayak, R., Vinayachandran, P., Nampoothiri, G., Almeida, A., et al. (2005). Hydrography of the eastern Arabian Sea during summer monsoon 2002. *Journal of Earth System Science*, *114*(5), 459–474. https://doi.org/10.1007/bf02702023

Singh, A. D., Jung, S. J., Darling, K., Ganeshram, R., Ivanochko, T., & Kroon, D. (2011). Productivity collapses in the Arabian Sea during glacial cold phases. *Paleoceanography*, *26*(3). https://doi.org/10.1029/2009pa001923

Sirocko, F., Garbe Schönberg, D., McIntyre, A., & Molfino, B. (1996). Teleconnections between the subtropical monsoons and high-latitude climates during the last deglaciation. *Science*, *272*(5261), 526–529. https://doi.org/10.1126/science.272.5261.526

Sirocko, F., Sarnthein, M., Erlenkeuser, H., Lange, H., Arnold, M., & Duplessy, J. C. (1993). Century-scale events in monsoonal climate over the past 24,000 years. *Nature*, *364*(6435), 322–324. https://doi.org/10.1038/364322a0

Smith, S. L., Codispoti, L. A., Morrison, J. M., & Barber, R. T. (1998). The 1994-1996 Arabian Sea Expedition: An integrated, interdisciplinary investigation of the response of the northwestern Indian Ocean to monsoonal forcing. *Deep-Sea Research II*, *45*, 1905–1915. https://doi.org/10.1016/s0967-0645(98)00075-7

Sonzogni, C., Bard, E., & Rostek, F. (1998). Tropical sea-surface temperature during the last glacial period: A view based on alkenones in Indian Ocean sediments. *Quaternary Science Reviews*, *17*, 1185–1201. https://doi.org/10.1016/s0277-3791(97)00099-1

Southon, J., Kashgarian, M., Fontugne, M., Metivier, B., & Yim, W. W.-S. (2002). Marine reservoir corrections for the Indian Ocean and southeast Asia. *Radiocarbon*, *44*(1), 167–180. https://doi.org/10.1017/s0033822200064778

Stuiver, M., Reimer, P. J., & Reimer, R. W. (2017). CALIB 7.1 [WWW program]. http://calib.org

Suthhof, A., Itekkot, V., & Gaye-Haake, B. (2001). Millenneal-scale oscillation of denitrification intensity in the Arabian Sea during the late Quaternary and its potential influence on atmospheric N_2O and global climate. *Global Biogeochemical Cycles*, *15*(3), 637–649. https://doi.org/10.1029/2000gb001337

Urey, H. C., Epstein, S., Lowenstam, H., & Emiliani, C. (1954). *Climatic history of the Earth by measuring the oxygen isotopic composition of the calcium carbonate in well-preserved marine fossils* (p. 23). Enrico Fermi Institute, The University of Chicago.

Versteegh, G. J. M., Bosch, H.-J., & de Leeuw, J. W. (1997). Potential palaeoenvironmental information of C_{24} to C_{36} mid-chain diols, keto-ols and mid-chain hydroxy fatty acids; a critical review. *Organic Geochemistry*, *27*(1–2), 1–13. https://doi.org/10.1016/s0146-6380(97)00063-6

Volkman, J. K., Barrett, S. M., & Blackburn, S. I. (1999). Eustigmatophyte microalgae are potential sources of C_{29} sterols, C_{22} - C_{28} *n*-alcohols and C_{28} - C_{32} *n*-alkyl diols in freshwater environments. *Organic Geochemistry*, *30*(5), 307–318. https://doi.org/10.1016/s0146-6380(99)00009-1

Volkman, J. K., Barrett, S. M., Dunstan, G. A., & Jeffrey, S. W. (1992). C_{30}-C_{32} alkyl diols and unsaturated alcohols in microalgae of the class *Eustigmatophyceae*. *Organic Geochemistry*, *18*(1), 131–138. https://doi.org/10.1016/0146-6380(92)90150-v

von Rad, U., Schulz, H., Riech, V., den Dulk, M., Berner, U., & Sirocko, F. (1999). Multiple monsoon-controlled breakdown of oxygen-minimum conditions during the past 30,000 years documented in laminated sediments off Pakistan. *Palaeogeography, Palaeoclimatology, Palaeoecology*, *152*(1–2), 129–161. https://doi.org/10.1016/s0031-0182(99)00042-5

Waelbroeck, C., Paul, A., Kucera, M., Rosell-Melee, A., Weinelt, M., Schneider, R., et al. (2009). Constraints on the magnitude and patterns of ocean cooling at the Last Glacial Maximum. *Nature Geoscience*, *2*(2), 127–132. https://doi.org/10.1038/Ngeo411

Wakeham, S. G., Peterson, M. L., Hedges, J. I., & Lee, C. (2002). Lipid biomarker fluxes in the Arabian Sea, with a comparison to the equatorial Pacific Ocean. *Deep-Sea Research Part II*, *49*(12), 2265–2301. https://doi.org/10.1016/s0967-0645(02)00037-1

Warnock, J. P., Bauersachs, T., Kotthoff, U., Brandt, H.-T., & Andrén, E. (2018). Holocene environmental history of the Ångermanälven Estuary, northern Baltic Sea. *Boreas*, *47*(2), 593–608. https://doi.org/10.1111/bor.12281

Webster, P. J., Magana, V. O., Palmer, T., Shukla, J., Tomas, R., Yanai, M., & Yasunari, T. (1998). Monsoons: Processes, predictability, and the prospects for prediction. *Journal of Geophysical Research: Oceans*, *103*(C7), 14451–14510. https://doi.org/10.1029/97jc02719

Wyrtki, K. (1971). *Oceanographic atlas of the international Indian Ocean expedition*. National Science Foundation.

Wyrtki, K. (1973). Physical oceanography of the Indian Ocean. In B. Zeitschel (Ed.), *The biology of the Indian Ocean* (pp. 18–36). Berlin: Springer. https://doi.org/10.1007/978-3-642-65468-8_3

Zhu, X., Jia, G., Mao, S., & Yan, W. (2018). Sediment records of long chain alkyl diols in an upwelling area of the coastal northern South China Sea. *Organic Geochemistry*. https://doi.org/10.1016/j.orggeochem.2018.03.014